Vol. 66: 211–228, 2015
doi: 10.3354/cr01348

CLIMATE RESEARCH
Clim Res

Published December 3

A coupled surface–subsurface modeling framework to assess the impact of climate change on freshwater wetlands

Xuan Yu[1], Gopal Bhatt[1], Christopher J. Duffy[1,*], Denice H. Wardrop[2], Raymond G. Najjar[3], Andrew C. Ross[3], Matthew Rydzik[3,4]

[1]Department of Civil and Environmental Engineering, The Pennsylvania State University, University Park, Pennsylvania 16802, USA
[2]Riparia, The Pennsylvania State University, University Park, Pennsylvania 16802, USA
[3]Department of Meteorology, The Pennsylvania State University, University Park, Pennsylvania 16802, USA
[4]Commodity Weather Group, Bethesda, Maryland 20814, USA

ABSTRACT: The Susquehanna River Basin (SRB) lies in the northeastern United States and contains a mosaic of wetlands that are susceptible to future climate change. This study develops a coupled surface–subsurface modeling framework to assess the prospects for the SRB wetlands under modified hydrologic processes induced by climate change. We selected 7 watersheds ranging in size from 163 to 902 km^2, representing the major landscapes of the SRB. We explored the broad spatial and temporal patterns across these watersheds between climate and wetland water levels by applying a coupled surface–subsurface model: Penn State Integrated Hydrologic Model (PIHM) with 7-yr hourly weather records from the North American Land Data Assimilation System. In the model calibration, we employed both streamflow and the spatial distribution of wetlands to constrain the model parameters. The possible effects of climate change on wetland hydrology were investigated by creating historical and future climate scenarios based on the output of one global climate model from Phase 3 of the Coupled Model Intercomparison Project (CMIP). We selected the best climate model based on historical performance to force the PIHM simulation of historical and future scenarios. The hydrologic scenarios suggested that water tables would fall, with greater declines in upland regions than in wetland areas. A key result of this study is that a high-resolution spatial and temporal model can resolve the heterogeneous wetland dynamics in the context of distributed mesoscale watershed modeling.

KEY WORDS: Climate change impacts · GCM · Spatial patterns · Watershed modeling · Water table · PIHM · Wetland · Susquehanna River Basin

1. INTRODUCTION

One of the recurring themes of research in environmental resources management is the preservation and sustainability of wetlands and their associated ecosystem services (Smardon 2009, Tiner 2002). However, our knowledge of the geospatial extent, behavior, and classification of wetlands is extremely limited due to their complex spatial scale and temporal dynamics (Tiner 2002, Wardrop et al. 2007b). From a hydrological view, it is generally recognized that shallow groundwater is a defining feature of many wetland types and can exert a strong control on plant and animal life, as well as on soil development (NRC 1995). The US National Research Council (NRC 1995, p. 50) concluded: 'The concept of wetland embraces a number of characteristics, including the elevation of the water table with respect to the ground surface, the

*Corresponding author: cxd11@psu.edu

duration of surface water, soil types that form under permanently or temporarily saturated conditions, and various types of plants and animals that have become adapted to life in a wet environment.' Tiner (2002, p. 21) stated: 'Wetland hydrology should be considered to be saturation within 30 cm of the soil surface for 2 wk or more during the growing season in most years (about every other year on average)'. More recently, US Federal authorities proposed new rules to define the waters of the United States, including the definition of a wetland as 'those areas that are inundated or saturated by surface or groundwater at a frequency and duration sufficient to support, and that under normal circumstances do support, a prevalence of vegetation typically adapted for life in saturated soil conditions' (US Army Corps of Engineers and EPA 2015, p. 37106). Clearly, the definitions of wetland explicitly incorporate a temporally dynamic understanding of a distributed variably saturated zone, which is not reported in many wetland assessment studies.

The National Wetlands Inventory (NWI) is the most readily available data source for mapping the location and spatial extent of wetlands throughout the United States (Martin et al. 2012), though it has limitations. A number of investigators have critiqued and attempted to improve the NWI database (Kudray & Gale 2000, Johnston & Meysembourg 2002, Ozesmi & Bauer 2002, Maxa & Bolstad 2009). These efforts to improve wetland maps and the underlying database have used remotely sensed, geospatial information (Maxa & Bolstad 2009) as well as geomorphological, biophysical, and hydrologic observations (Wardrop et al. 2007b) to establish and map a variety of wetland types on a watershed basis. It is generally agreed that quantitative hydrologic characteristics are among the most important factors in wetland identification, delineation, classification, and evaluation (Johnson et al. 2004, Wardrop et al. 2007b, McLaughlin et al. 2014, Fossey et al. 2015).

Clearly, geospatial classification of specific wetland types and their relation to shallow groundwater-stream conditions across the watershed provide a valuable tool for resource assessment, and the close relationship of these specific wetland types to shallow groundwater suggests that they may, in turn, also play a useful role in watershed modeling studies. Traditional watershed modeling has focused primarily on streamflow simulation (Pyzoha et al. 2008, Su et al. 2000, Yuan et al. 2011), with limited attention paid to understanding spatial patterns of hydrological responses and temporal patterns of lateral groundwater flow (Grayson et al. 2002). More recently, advances in the representation of hydrologic processes have substantially improved the fidelity of spatial simulations. Many modeling groups now use geospatial data for terrain, vegetation, soil, and geology as the basis for a complete representation of groundwater dynamics, stream-aquifer interactions, and channel/floodplain routing (Mirus & Loague 2013, Golden et al. 2014, Clark et al. 2015). A question we attempt to answer here is: Can distributed watershed models utilize the NWI as a data source for constraining surface-groundwater conditions (Lu et al. 2009, Min & Wise 2009, Scibek & Allen 2006)?

Within the Chesapeake Bay watershed, climate variability has influenced, and is expected to continue to influence, environmental changes in the Bay itself (Neff et al. 2000, Rogers & McCarty 2000, Najjar et al. 2009). Statistical analysis suggests that a 3°C increase in mean annual temperature may be associated with a stronger drought response in the mid-Atlantic United States. Although concomitant increases in precipitation may mitigate part of the likely water shortage (Huntington 2003), it is also reasonable to assume that freshwater wetlands would be vulnerable to climate change under these conditions (Najjar et al. 2010, Wardrop et al. 2007a). Located within the Chesapeake Bay watershed, the Susquehanna River Basin (SRB) encompasses an area of 71 225 km^2, of which 76% is in Pennsylvania, 23% in New York, and 1% in Maryland. Over 90% of the basin is underlain by flat-lying sedimentary rock strata of the Appalachian Plateau Physiographic Province. The principle tributaries are the Susquehanna (747 km), the West Branch of the Susquehanna (391 km), and the Juniata (167 km). Approximately 90% of the freshwater inputs to the Upper Chesapeake Bay and 50% to the entire Chesapeake Bay are from the Susquehanna. Groundwater is by far the largest store of water in the Basin, serving 50% of the water users. Groundwater recharge, discharge (baseflow), and shallow groundwater storage are highly sensitive to climate conditions (Fan et al. 2013, Green et al. 2011, Taylor et al. 2013, Kløve et al. 2014). The timing and magnitude of drought conditions depend on the space and time scales of groundwater storage. Recently, the assessment of climate change impacts and management practices on watershed resources was the focus of a comprehensive multidisciplinary study (Brooks & Wardrop 2013, Zhang et al. 2010).

In this study, we examine the spatial response of shallow groundwater conditions of specific wetland types to climate change for 7 mesoscale watersheds of the SRB, ranging in size from 163 to 902 km^2. Our first objective is to test the ability of a coupled surface–subsurface hydrologic model to capture spa-

tial shallow water table dynamics. In the model, the spatial heterogeneity of the watersheds is explicitly resolved in the watershed responses, which should improve our understanding from streamflow to landscape scale. The second objective is to project how future climate changes would affect the watershed response in terms of total water budget and local spatial hydrologic dynamics. The methodological steps of the study are (1) calibration and evaluation of a coupled surface–subsurface, spatially distributed hydrologic model utilizing NWI data as a constraint on the water table over each watershed; (2) use of the model simulation during 2004 to 2010 to extract wetland locations and distribution; and (3) examination of the sensitivity of basin-scale and distributed hydrologic response under future climate change using the best climate scenario.

2. DESCRIPTION OF STUDY AREA

The 7 watersheds in this study are shown in Fig. 1 and their characteristics are listed in Tables 1 & 2. A brief description of each watershed follows.

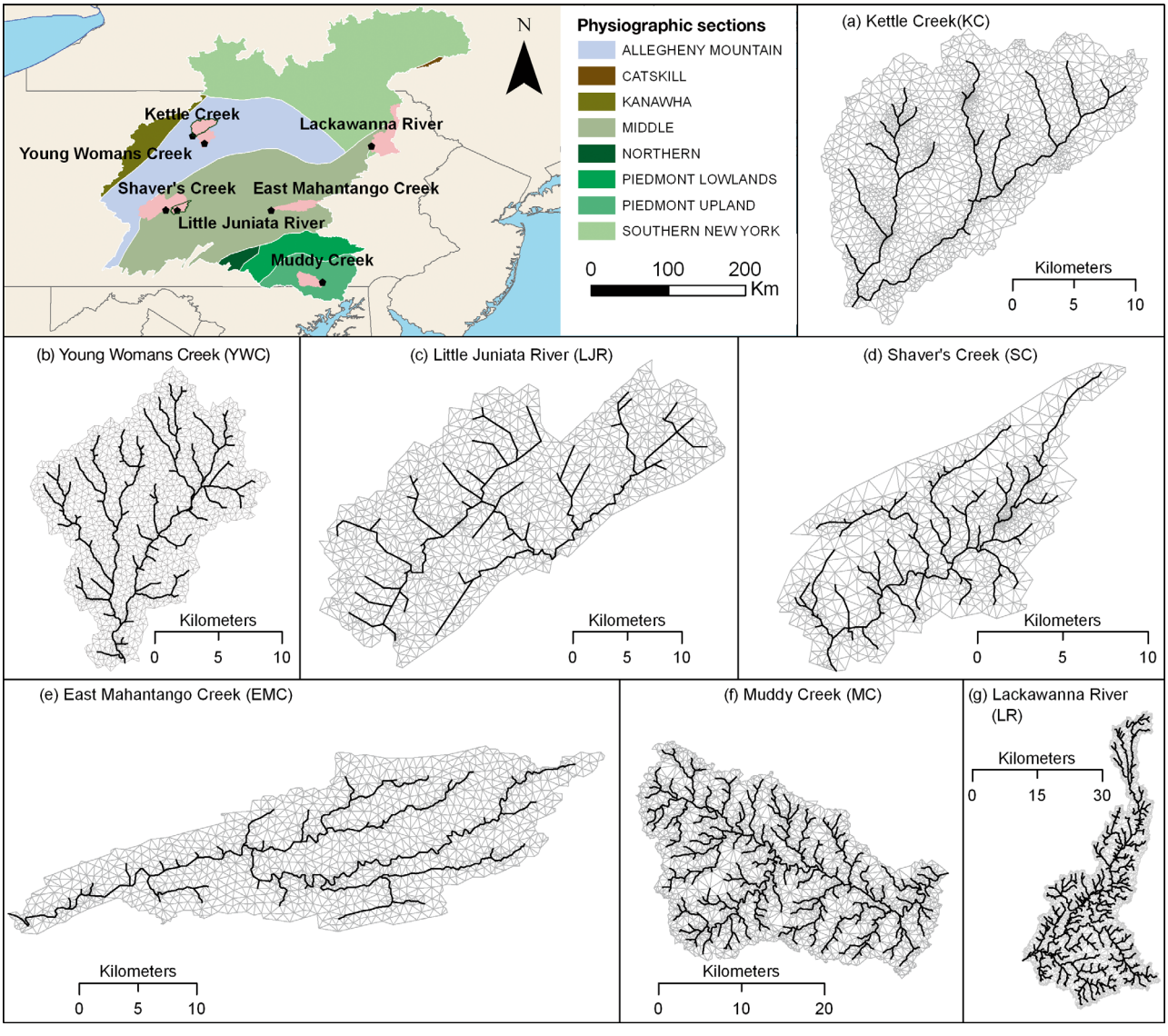

Fig. 1. Large-scale map: location and areas (pink) of the 7 watersheds in the Susquehanna River Basin (SRB) in the northeastern United States used to model the impacts of climate change on freshwater wetlands. The boundaries of Kettle Creek and Little Juniata River are outlined to demarcate them from adjacent watersheds. Subplots (a–g) show the Penn State Integrated Hydrologic Model (PIHM) grid for each watershed. PIHM uses triangle mesh (gray) to represent the watershed, and linear segment (black) to represent the stream channel

Table 1. The 7 watersheds in the Susquehanna River Basin (SRB) in the northeastern United States used to model the impacts of climate change on freshwater wetlands and details of corresponding USGS gauges

	Watershed name	Modeling area (km^2)	USGS gauge			
			ID	LAT	LON	Drainage area (km^2)
KC	Kettle Creek	355.44	01544500	41.4758	–77.8261	352.2
YWC	Young Womans Creek	230.70	01545600	41.3894	–77.6911	119.7
LJR	Little Juniata River	843.26	01558000	40.6125	–78.1408	569.8
SC	Shaver's Creek	162.71	01558500	40.6106	–78.0072	120.2
EMC	East Mahantango Creek	422.37	01555500	40.6111	–76.9122	419.6
MC	Muddy Creek	360.50	01577500	39.7725	–76.3161	344.5
LR	Lackawanna River	902.03	01536000	41.3592	–75.7447	859.9

Table 2. Percentage of land cover classes in each watershed. Source: National Land Cover Database (NLCD 92) land cover descriptions (http://landcover.usgs.gov/classes.php). Parentheses: NLCD 92 land cover class ID codes

	Wetland (91, 92)	Forest (41, 42, 43)	Developed (21, 22, 23)	Agricultural (81, 82, 85)
KC	0.23	85.32	0.12	13.98
YWC	0.15	98.78	0.10	0.61
LJR	0.40	72.03	1.75	25.61
SC	0.78	70.64	0.16	28.39
EMC	0.65	53.76	1.27	43.06
MC	1.08	33.06	0.39	64.68
LR	4.04	70.09	14.58	9.20

(*a*) *Kettle Creek*. Kettle Creek (KC) is a tributary of the West Branch of the Susquehanna River, which has a drainage area of 352.2 km^2. Overall, land cover in the watershed is categorized as 85.32% forest and 13.98% agriculture.

(*b*) *Young Womans Creek*. Young Womans Creek (YWC) is another tributary of the West Branch of the Susquehanna River, encompassing an area of 119.7 km^2. Heavy forest covers 98.78% of the watershed.

(*c*) *Little Juniata River*. The Little Juniata River (LJR) is a tributary of the Juniata River, the second-largest tributary of the Susquehanna River. The drainage area is 569.8 km^2. The land cover of the LJR is 72.02% forest and 25.61% agriculture.

(*d*) *Shaver's Creek*. Shaver's Creek (SC) is located southeast of LJR. The drainage area is 120.2 km^2. The land use in the valleys of SC is mixed, primarily, with farming (28.39%) and significant amounts of forests (70.64%) that cover the run along the ridges.

(*e*) *East Mahantango Creek*. East Mahantango Creek (EMC) is located in east-central Pennsylvania, with a drainage area of 419.6 km^2. The land cover is characterized by being predominantly forested (53.76%) at ridge tops with agriculture (43.06%) dominating the valley floors.

(*f*) *Muddy Creek*. Muddy Creek (MC) is a tributary of the Susquehanna River in York County, PA. The drainage area is 344.5 km^2. MC watershed represents an intensive farming watershed, with agricultural land covering 65.68%.

(*g*) *Lackawanna River*. The Lackawanna River (LR) is the largest tributary to the North Branch of the Susquehanna River in Northeastern Pennsylvania. The drainage area is 859.9 km^2. The land cover is predominantly forest (70.09%) and urban area (14.58%).

3. MATERIALS AND METHODS

3.1. Coupled surface–subsurface hydrological modeling

The Penn State Integrated Hydrologic Model (PIHM) is a coupled surface–subsurface, spatially distributed, hydrologic model. It simulates the terrestrial water cycle, including interception, throughfall, infiltration, recharge, evapotranspiration, overland flow, unsaturated soil water, groundwater flow, and channel routing, in a fully coupled scheme (Qu & Duffy, 2007). Evapotranspiration is calculated using the Penman-Monteith approach adapted from Noah_LSM (Chen & Dudhia, 2001), which resolves the land surface energy balance with specific meteorologic conditions. Overland flow is modeled using a 2-D estimation of the St. Venant equations. Movement of moisture in unsaturated zones is assumed to be vertical only (1-D), which is modeled using Richard's equation. When the moisture recharges into saturated zone, the water can flow laterally; lateral flow is governed by the continuity equation and Darcy's law. The model assumes that each subsurface layer can have both unsaturated and saturated storage components. Balance equations of the unsaturated and saturated zones are formed in a fully coupled way. Channel routing is modeled using a 1-D estimation of the St. Venant equations. Spatially, the modeling domain is decomposed into Delaunay triangles. The

resolution of the triangular mesh allows users to customize according to the geomorphological or hydrological characteristics of the watershed. Also, the triangles can be constrained by point observations (e.g. streamflow, groundwater level, soil moisture, and leaf area index), and the watershed boundary conditions (Kumar 2009). The model resolves hydrological processes for land surface energy, overland flow, channel routing, and subsurface flow, governed by a partial differential equation (PDE) system. The system is discretized on the triangular mesh and on projected prisms from canopy to bedrock. The model also includes canopy interception, evapotranspiration, infiltration, and recharge within the fully coupled system. PIHM uses a semi-discrete, finite-volume formulation for solving the system of coupled PDEs, resulting in a system of ordinary differential equations (ODEs) representing all processes within the prismatic control volume. The local system is assembled throughout the model entire domain, and the global ODE system is solved using the CVODE implicit solver (Cohen & Hindmarsh 1996). Detailed descriptions of the modeling theory and mathematical formulation can be found at the PIHM website (www.pihm.psu.edu) and associated publications (Kumar 2009, Qu & Duffy 2007).

Advantages of PIHM for simulating wetland hydrology are: (1) the space-time patterns of the water table can be explicitly simulated across the basin; and (2) using the PIHMgis (Bhatt et al. 2014) tool, the spatial simulated wetland can be compared and resolved with the NWI dataset. An important result of the study is that high-resolution, coupled surface–subsurface models can be used for establishing a scientific basis for the evaluation of environmental change and the impact on ecosystem services.

3.2. Climate scenarios for SRB

The possible effects of climate change on wetland hydrology were investigated by creating historical and future climate scenarios based on the output of one global climate model from Phase 3 of the Coupled Model Intercomparison Project (CMIP3) (Meehl et al. 2007). The historical scenario in this study is based on years 1979–1998 from the 20th century experiment (20C3M), and the future scenario is based on years 2046–2065 from the SRES A2 emissions experiment.

Because differences among climate models account for much of the spread in future climate projections, it is preferred to use multiple climate models when projecting the impact of future climate change (Chien et al. 2013, Masood et al. 2015). However, computational resource limitations in running PIHM forced us to select a single model for the wetland impact assessment.

To select the best climate model, we analyzed daily output from the 12 CMIP3 climate models listed in

Table 3. List of selected climate models from Phase 3 of the Coupled Model Intercomparison Project 3 (CMIP3)

Originating group(s)	Country	CMIP3 I.D.	Reference
Bjerknes Centre for Climate Research	Norway	BCCR-BCM2.0	Furevik et al. (2003)
Canadian Centre for Climate Modelling & Analysis	Canada	CGCM3.1(T47)	Flato & Boer (2001)
Météo-France; Centre National de Recherches Météorologiques	France	CNRM-CM3	Salas-Mélia et al. (2005)
CSIRO Atmospheric Research	Australia	CSIRO-Mk3.0	Gordon et al. (2002)
CSIRO Atmospheric Research	Australia	CSIRO-Mk3.5	
Max Planck Institute for Meteorology	Germany	ECHAM5/ MPI-OM	Jungclaus et al. (2006)
Meteorological Institute of the University of Bonn; Meteorological Research Institute of Korea Meteorological Administration (KMA); Model and Data group	Germany / Korea	ECHO-G	Legutke & Voss (1999)
US Dept. of Commerce; NOAA; Geophysical Fluid Dynamics Laboratory	USA	GFDL-CM2.0	Delworth et al. (2006)
US Dept. of Commerce; NOAA; Geophysical Fluid Dynamics Laboratory	USA	GFDL-CM2.1	Delworth et al. (2006)
Institute for Numerical Mathematics	Russia	INM-CM3.0	Diansky & Volodin (2002)
Center for Climate System Research (The University of Tokyo); National Institute for Environmental Studies; Frontier Research Center for Global Change of the Japan Agency for Marine-Earth Science and Technology (JAMSTEC)	Japan	MIROC3.2 (medres)	K-1 Model Developers (2004)
Meteorological Research Institute	Japan	MRI-CGCM2.3.2	Yukimoto et al. (2001)

Table 3, using a ranking method similar to that of Reichler & Kim (2008), who developed an error index based on the ability of general circulation models (GCMs) to simulate the spatial distribution of several climate variables. Here, we focus on the ability of each model to reproduce the observed annual cycles of 3 basic metrics each for temperature and precipitation: (1) the climatological monthly mean value, (2) the standard deviation of the monthly mean value (a metric of interannual variability), and (3) the climatological standard deviation within each month (a metric for sub-monthly variability). Each model has multiple realizations, using the same boundary conditions but different initial conditions. Before determining the rankings, the first realization for each model was selected, and the output of each model was linearly interpolated to a 1° grid covering the watersheds (Fig. 2). Following Reichler & Kim (2008), the error index for an individual GCM (g, a total of 12) and variable (v, a total of 6) was calculated by:

$$e^2_{v,g} = \sum_n \sum_m \frac{(\overline{s}_{v,g,m,n} - \overline{o}_{v,m,n})^2}{\sigma^2_{v,m,n}} \quad (1)$$

where n denotes a 1° grid point, m denotes month (January to December), $\overline{s}$ and $\overline{o}$ respectively represent the model and observed annual cycle, and σ^2 is the interannual variability of the observed monthly means. Observations from the University of Delaware monthly-mean temperature and precipitation dataset (http://climate.geog.udel.edu/~climate/html_pages/archive.html) were used for the mean and interannual variability of temperature and precipitation, and the North American Regional Reanalysis (NARR) (Mesinger et al. 2006) was used for sub-monthly variability of temperature and precipitation. Both of these products were interpolated to the same 1° grid as the GCMs. Next, for each variable, each GCM error index was divided by the model mean error index over the ensemble of GCMs for the given variable:

$$I^2_{v,g} = \frac{e^2_{v,g}}{\overline{e^2_{v,g}}^{g}} \quad (2)$$

This scales the error indices so that they each vary around 1, with models with above-average performance <1 and those with below-average performance >1. Finally, for each model, the overall error index used to rank the model is an average over the scaled error index of each variable:

$$I^2_g = \overline{I^2_{v,g}}^{v} \quad (3)$$

As a result, models with monthly climatologies that closely match the observed climatology have a lower error index, and a perfect model would have an error index of zero. Following Reichler & Kim (2008), 95% confidence intervals for each ranking were also derived by recalculating the error index after resampling the values used to calculate the mean of each month in the observed climatology of each variable. We used bootstrap resampling with 1000 samples. The error indices are shown in Fig. 3. The rankings indicate that the MRI-CGCM2.3.2 model is the best-performing model.

After identifying the MRI-CGCM2.3.2 as the best-performing climate model, daily output from this model (surface temperature, precipitation, downwelling solar radiation, specific humidity, and wind speed) was prepared for use in PIHM by applying bias correction. The regridded NARR product was used to determine bias in temperature and precipitation. Biases in wind and humidity were determined from an average of observations at 7 Automated Surface Observing System stations within the Susquehanna River Basin from 1999 to 2009. Bias in downwelling solar radiation was determined from measurements at the Surface Radiation station at The Pennsylvania State University near State College, Pennsylvania. These products were not interpolated to the GCM grid.

Daily mean temperature and total precipitation were bias corrected using equidistant and equiratio cumulative distribution function (CDF) matching, respectively (Li et al. 2010, Wang & Chen 2014). For historical scenario data, the bias correction pro-

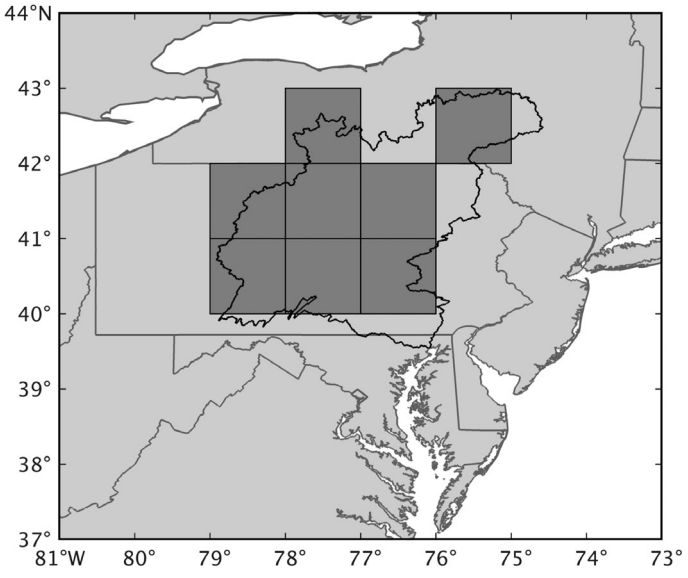

Fig. 2. The General Circulation Model (GCM) interpolation grid for the approximation of entire Susquehanna River Basin (SRB). The area of the SRB is outlined in black. The 8 dark-gray tiles are the areas selected for the interpolation of climate projections

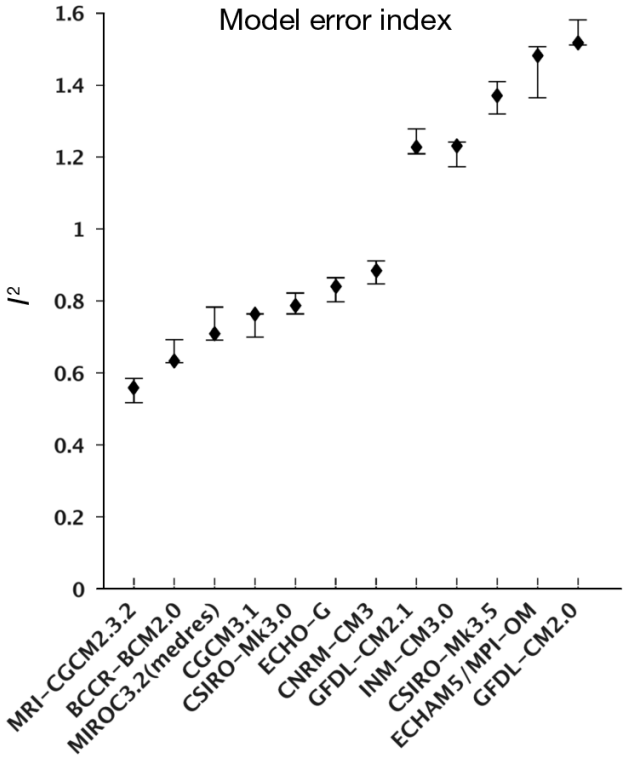

Fig. 3. Temperature and precipitation error index (I^2) of 12 CMIP3 climate models (see Table 3). Better models have a lower error index. Error bars indicate 95 % confidence regions

duces a time series with the same CDF as the observed time series. For future scenario data, the CDF of the corrected data is the CDF of the model future data shifted by the mismatch between the modeled historical and observed CDFs. This corrects the model bias while still allowing the shape of the data distribution to change from the historical to the future period. Mathematically, using the same notation as Wang & Chen (2014), the correction applied to temperature was

$$\tilde{x}_{m-p.adjust.} = x_{m-p} + F_{o-c}^{-1}[F_{m-p}(x_{m-p})] - F_{m-c}^{-1}[F_{m-p}(x_{m-p})] \quad (4)$$

where x_{m-p} is a value from the model during the prediction period (either the historical or future), F_{m-p} is the CDF of the model prediction data, F_{o-c}^{-1} is the inverse CDF of the current observed data, and F_{m-c}^{-1} is the inverse CDF of the model data during the current (historical) period. The CDF is the empirical cumulative distribution function, which is defined as:

$$F(x) = \frac{\text{number of sample values} \le x}{\text{number of samples}}$$

The inverse CDF is then just $x(F)$.

An additive adjustment could cause precipitation to be corrected to below zero. Instead, precipitation was adjusted using a multiplicative scaling factor:

$$x_{m-p.adjust.} = x_{m-p} \times \frac{F_{o-c}^{-1}[F_{m-p}(x_{m-p})]}{F_{m-c}^{-1}[F_{m-p}(x_{m-p})]} \quad (5)$$

The CDFs were calculated and shifted separately for each month in the calendar year to allow for the bias and projected change in the model to change throughout the year. For example, spring and fall months may have similar temperatures but different biases and projected changes.

Daily mean downwelling solar radiation, specific humidity, and wind speed were corrected using a simple scaling method that applies the same multiplicative shift to the current and future data. To apply the correction, each variable is multiplied by the ratio of the observed mean of the variable to the model historical mean. This method corrects the mean but not the higher-order statistics. Separate scaling factors were calculated and applied for each variable, grid point, and month of the calendar year.

After performing the bias correction, spatially uniform, daily meteorological conditions for the hydrological model were generated by selecting data from one GCM grid cell near the center of the watersheds to retain temporal variability (for precipitation) and by averaging the model output over all of the grid cells (remaining variables). Finally, specific humidity was converted to relative humidity and vapor pressure.

The resulting historical and future scenarios of climatological input data are shown in Fig. 4. Overall, annual total precipitation amounts increase slightly from the historical scenario to the future scenario. Annual mean temperature increases, and both extreme high and low temperatures increase. Average vapor pressure increases, but average relative humidity decreases slightly as a result of significantly higher temperatures. Finally, both wind speed and solar radiation are slightly higher and more variable in the future scenario.

3.3. Proposed methodology

In principal, distributed watershed hydrologic modeling attempts to capture all the hydrological processes and predicted different hydrological state variables and fluxes within an integrated modeling framework. Of particular focus here is the coupled surface–subsurface response across the catchment. Limited spatial water-table depth data were avail-

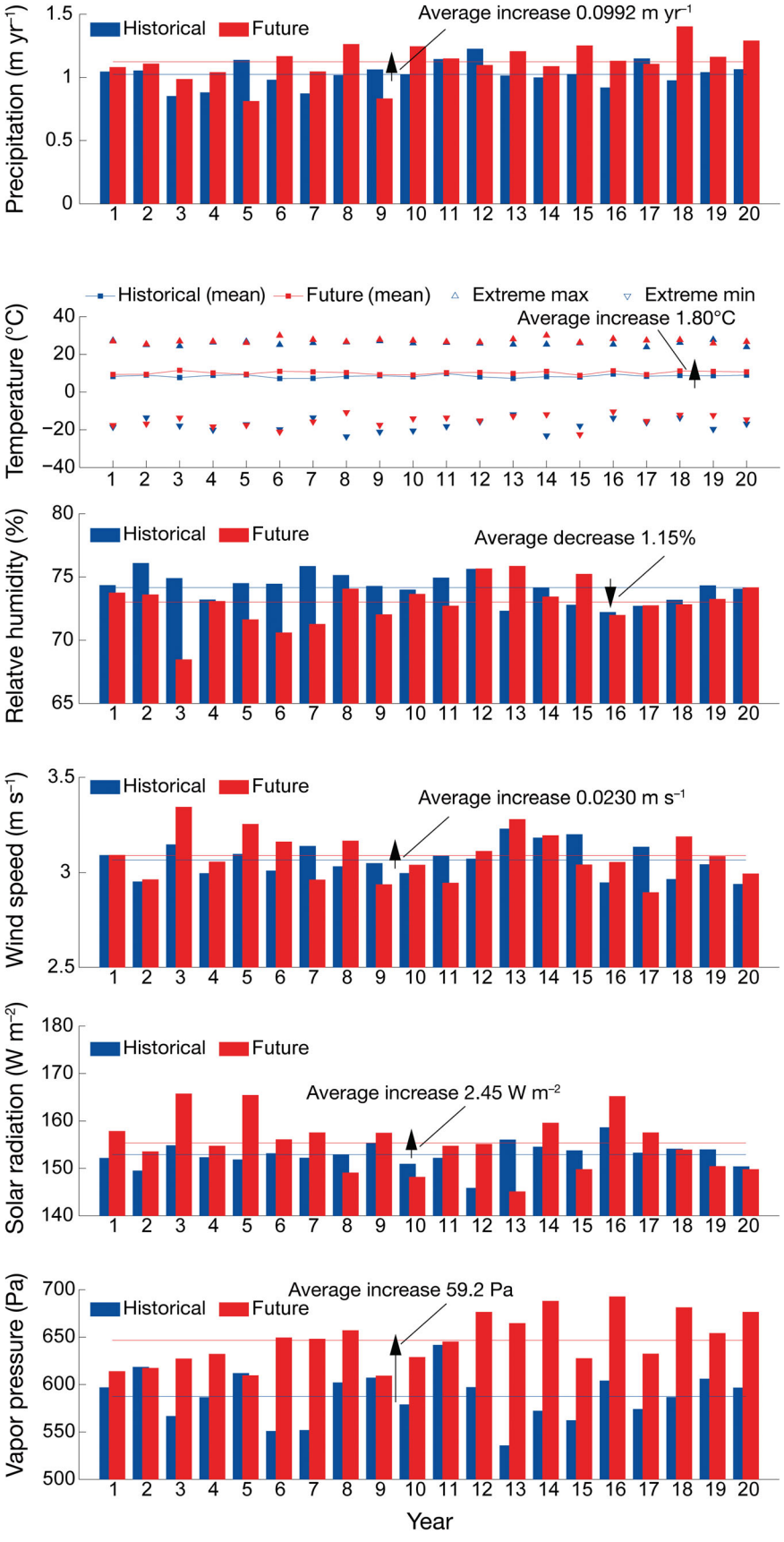

Fig. 4. Annual mean time series of climatological inputs to the hydrological model for the historical (1979–1998) (blue) and future (2046–2065) (red) scenarios. Horizontal lines (for temperature, the lines are not straight) show the average across time for each scenario

able, and the NWI maps were used to constrain the water table during calibration (e.g. all wetlands depicted in the NWI in this area are non-tidal, thus are defined as having a water table within 30 cm of the surface for at least part of the year). US Geological Survey (USGS) streamflow data provide another constraint in the optimization process. The procedure includes the following steps: (1) assign PIHM modeling parameters from national data sets for land cover, soils, hydrogeology, and topography; (2) calibrate the model by following the method of Yu et al. (2013) with the constraints of streamflow time series and the NWI spatial map; and (3) assess wetland responses to the downscaled climate change scenario.

3.4. Model data setup and parameter calibration

We applied PIHM at each watershed. The model input data included spatial information on land cover, soil, and geology, which were derived from national databases (Yu et al. 2013). PIHM has a tightly coupled GIS tool called PIHMgis (Bhatt et al. 2014) to discretize the watershed and then overlay the GIS layer with the computational mesh. The model data preparation processes for KC are illustrated in Fig. 5. The soil, vegetation, and topography parameters were estimated by overlapping national data with the model mesh. Also the hourly

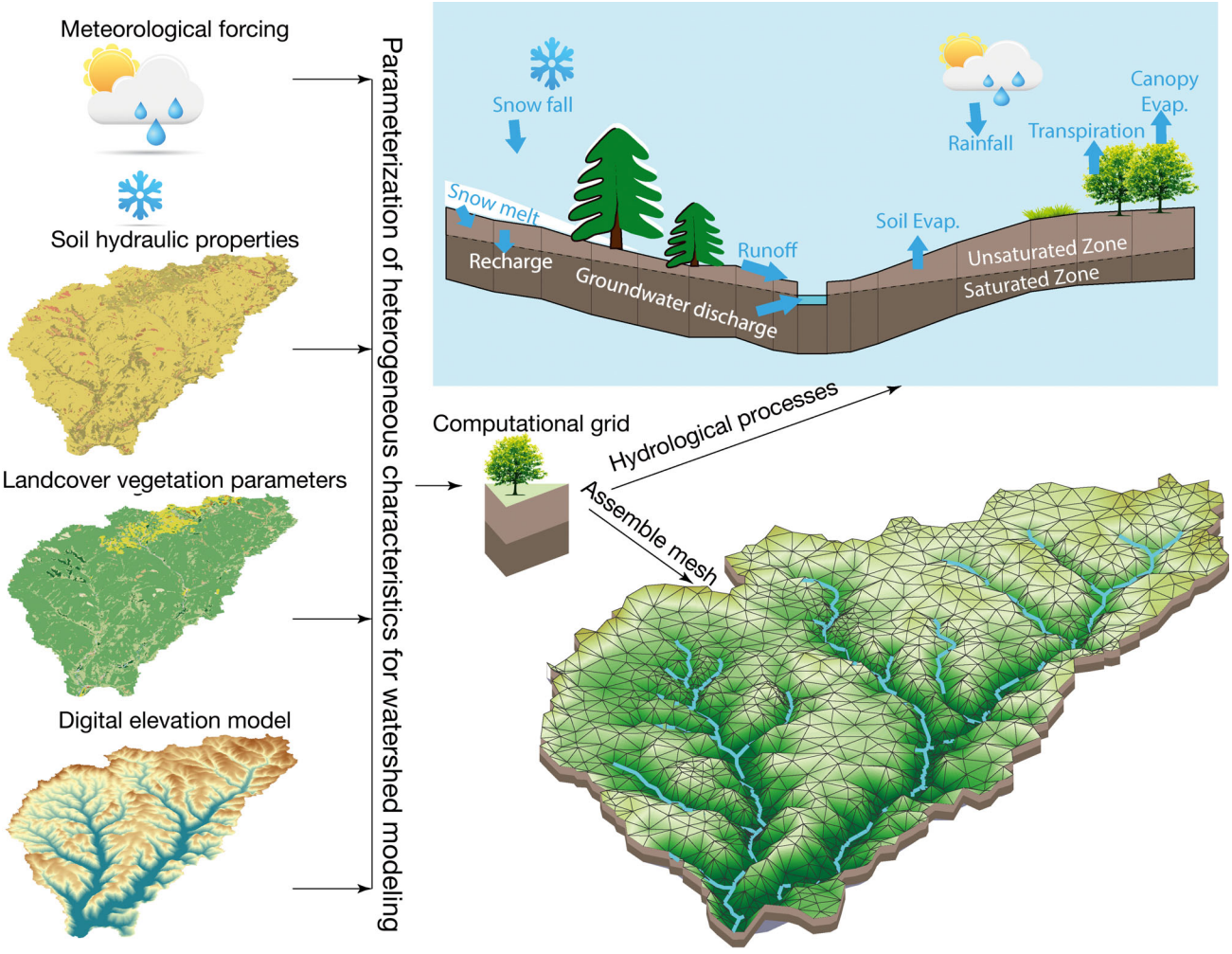

Fig. 5. The PIHM model data setup processes. The domain of Kettle Creek is used to illustrate the model data preparation, model processes, and spatial model mesh representation

meteorological forcing from NLDAS-2 (NASA, 2013) was assigned to the model mesh. Similarly, all other watersheds were processed for PIHM modeling. The resolution and other metrics of the mesh for each watershed are listed in Table 4.

Table 4. PIHM modeling mesh resolution

Watershed	Modeling area (km^2)	No. of triangles in the mesh domain	No. of channels in the mesh domain	Spatial modeling resolution (km^2)
KC	355.44	3098	342	0.115
YWC	230.70	3172	651	0.073
LJR	843.26	2089	264	0.404
SC	162.71	1986	414	0.082
EMC	422.37	2606	509	0.162
MC	360.50	4779	1399	0.075
LR	902.03	5355	1521	0.168

In previous studies, PIHM was manually calibrated (Kumar et al. 2013) based on a relaxation experiment designed to capture the drying soil matrix and macro hydraulic properties (porosity and conductivity) and the baseflow recession to the stream reach. To reduce the labor in model calibration, an evolutionary algorithm Covariance Matrix Adaptation Evolution Strategy (CMA-ES; Hansen & Ostermeier, 2001) was introduced for PIHM parameter optimization (Yu et al. 2013). The new calibration process partitions PIHM parameters into 2 groups: the first group of parameters generally describes hydrologic processes influenced by hydrologic events and is calibrated by CMA-ES, while the

second group of parameters is largely influenced by seasonal changes in energy and is calibrated using the annual water budget. In this study, we used both streamflow and water table depth as estimated by NWI to constrain the model. The NWI map was overlaid on the model domain, and NWI wetlands were identified. For each triangle that includes a wetland, the average of simulated groundwater depth was constrained to be <0.3 m below the land surface. Also, daily streamflow time series were used to calibrate the soil and subsurface hydrologic parameters. The calibration objective was formulated as:

$$e = 1 - \mathrm{NSE}_{\mathrm{streamflow}} + \sqrt{\frac{1}{n}\sum_{i=1}^{n}(\mathrm{GW}_i - 0.3)^2} \quad (6)$$

where e is the objective function, $\mathrm{NSE}_{\mathrm{streamflow}}$ is the Nash-Sutcliffe model efficiency coefficient (Nash & Sutcliffe 1970) of streamflow, n is the number of triangles with maximum water table depth >0.3 m and overlapping with NWI maps, and GW_i is the corresponding maximum water table depth. The event-based calibration time period (Yu et al. 2013) was a 2 wk temporal window with at least 1 flooding event during the growing season (from May to September) in 2004. To minimize the initial condition impact (Qu & Duffy 2007), we ran the model for another 1 mo period in advance as spin-up. We only calculated the objective function using the hydrologic variables during the 2 wk temporal window after the spin-up. The seasonal-scale calibration period (Yu et al. 2013) was the entire year of 2004. The calibration results are listed in the Supplement at www.int-res.com/articles/suppl/c066p211_supp.pdf.

The statistical criteria used to evaluate PIHM performance included mean error (ME), Pearson's correlation coefficient (R), and NSE (Nash & Sutcliffe 1970). ME is commonly used to evaluate the average systematic error among the simulated and the observed values. Negative values of ME indicate model under-estimation, while positive values correspond to over-estimation. R is a measure of the strength of the association between observed and predicted values and may take any value between −1 and 1. NSE varies from minus infinity to 1.0, with higher values indicating better agreement.

$$\mathrm{ME} = \frac{\overline{P} - \overline{O}}{\overline{O}} \quad (7)$$

$$R = \frac{\sum_{i=1}^{t}(O_i - \overline{O})(P_i - \overline{P})}{\sqrt{\sum_{i=1}^{t}(O_i - \overline{O})^2}\sqrt{\sum_{i=1}^{t}(P_i - \overline{P})^2}} \quad (8)$$

$$\mathrm{NSE} = 1 - \frac{\sum_{i=1}^{t}(O_i - P_i)^2}{\sum_{i=1}^{t}(O_i - \overline{O})^2} \quad (9)$$

where O_i is observed variable at time i, P_i is model simulated variable at time i. $\overline{O}$ and $\overline{P}$ are the mean of observed and simulated variable.

In this study, we explore the prospect that climate change in the region may result in water table responses that might affect wetland extent and function across the SRB. The distribution of groundwater level responses was classified into wetland, upland, and other categories to examine the spatial heterogeneity of the climate change impacts. Specifically, the PIHM simulation identifies the wetland triangles, and then categorizes the rest of the triangles: if the drainage area of a triangle is <10% of the whole watershed, the triangle is classified as the 'upland'; the remaining triangles are classified as the others'.

4. RESULTS

4.1. Model simulation

The simulated and observed streamflow are plotted in Fig. 6 and model performance is listed in Table 5, including ME, R, and NSE criteria for daily streamflow. Using the criteria of NSE > 0.50 and ME < ±25% (Moriasi et al. 2007) as satisfactory, the performance of simulated daily streamflows were all found to have NSE > 0.50, except LR. All NSE metrics were lower during the 6-yr (2005–2010) validation, again using daily streamflows. Simulations for 2 watersheds (KC and LR) were deemed unsatisfactory during the validation period with NSE < 0.36 (Moriasi et al. 2007).

Using simulated daily water table depth from 2004 to 2010, we evaluated the dynamic wetland area over the growing season using a definition for a wetland as 'having a water table depth <0.3 m for >2 wk during the period from May to September'. As expected, the model is able to identify the location of the majority of NWI wetlands during the simulation (Table 6, Fig. 7), since wetlands were used as a spatial constraint on the depth to groundwater during calibration. The identification rate of NWI wetlands ranges from 73 to 98%. It is interesting to note that the model-predicted wetland area is significantly larger than NWI wetland area (Table 6). The over-prediction rate ranges from 5.4 to 25.0%. This suggests either that hydrologic modeling with high-resolution terrain produces false positives or that the model can explicitly reveal additional potential wetland locations, which are not constrained during the calibra-

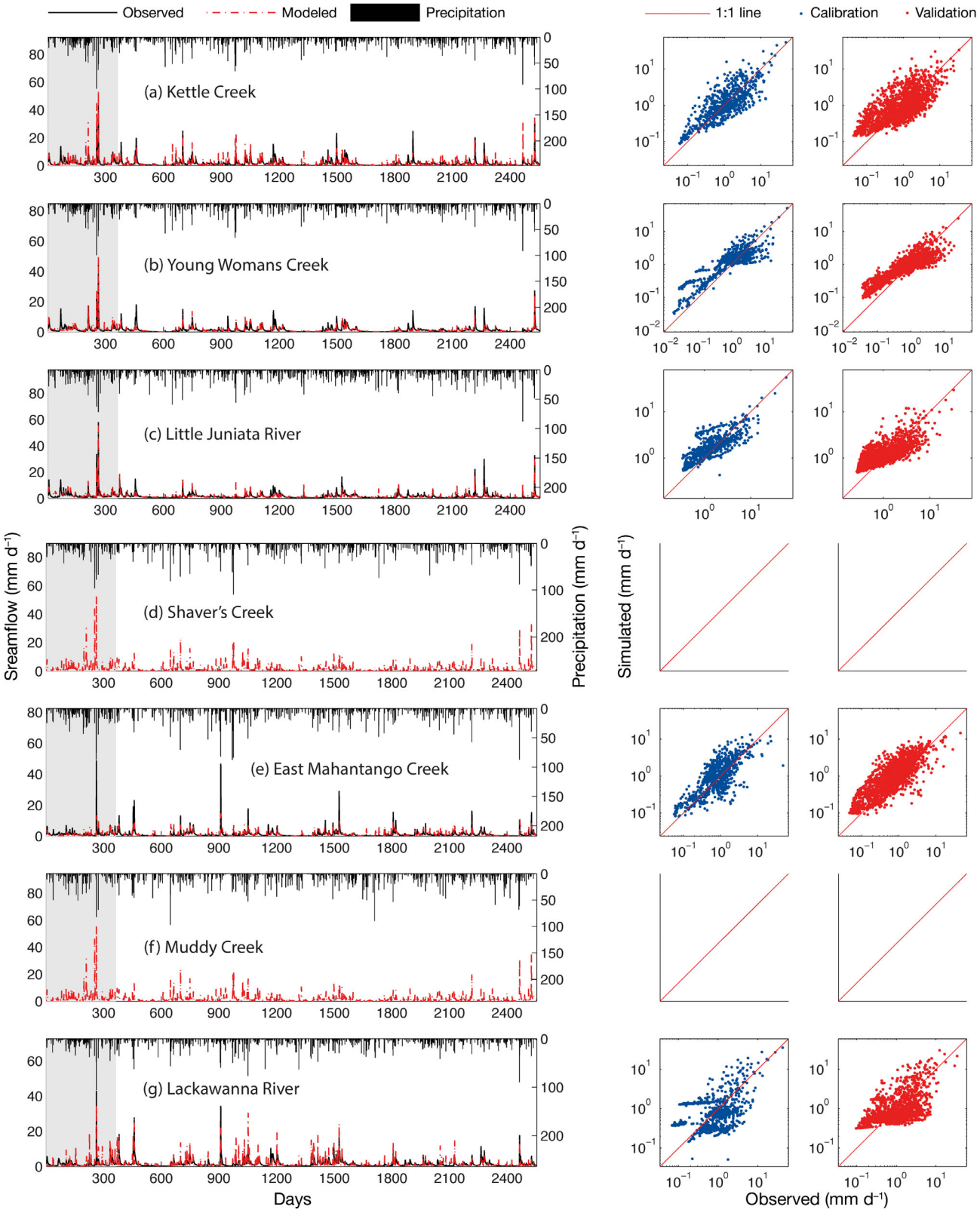

Fig. 6. Observed and simulated streamflow (2004–2010) at the 7 watersheds. First column: hydrographs. Gray: calibration period (2004); unshaded: validation period (2005–2010). The second and third columns show simulated versus observed streamflow during the calibration period and validation period, respectively. Note that USGS gauges for Shaver's Creek and Muddy Creek do not have data available for 2004 to 2010

Table 5. PIHM performance in daily streamflow simulation during calibration (2004) and validation (2005–2010) periods. N/A: not available

Watershed	Mean error (%)		Pearson's correlation coefficient		Nash–Sutcliffe coefficient of efficiency	
	Calibration	Validation	Calibration	Validation	Calibration	Validation
KC	–1.70	4.88	0.84	0.66	0.55	0.33
YWC	–2.82	–11.7	0.80	0.68	0.65	0.45
LJR	8.02	–3.63	0.89	0.77	0.79	0.58
SC	N/A	N/A	N/A	N/A	N/A	N/A
EMC	3.15	21.94	0.63	0.67	0.56	0.43
MC	N/A	N/A	N/A	N/A	N/A	N/A
LR	–9.48	–4.66	0.77	0.65	0.36	0.21

Table 6. PIHM performance in wetland area identification

Watershed	(A) NWI wetland area (km^2)	(B) PIHM predicted wetland area (km^2)	(C) Wetland overlapping with PIHM prediction (km^2)	(D) Identification rate (C/A) (%)	(E) Over-prediction rate (B/A) (%)
KC	0.82	5.70	0.73	88	6.9
YWC	0.35	6.03	0.32	93	17.3
LJR	3.37	53.59	3.29	98	15.9
SC	1.28	22.74	1.09	86	17.8
EMC	2.75	68.75	2.02	73	25.0
MC	3.89	45.90	3.07	79	11.8
LR	36.47	197.26	32.89	90	5.4

tion. There is qualitative evidence to suggest that the latter is most likely case at least for the SC watershed where fieldwork indicates many more actual wetlands than listed in the NWI.

4.2. Hydrologic responses

The future climate in Pennsylvania was predicted to increase in both temperature and precipitation, though the relationship is complex. The simulation suggested that future climate change increases evapotranspiration and streamflow in the all the watersheds. The combined effects cause the decline of the basin-averaged groundwater table elevation (Table 7).

The local responses are classified into 5 groups (according to the overall distribution of the water table change): < –0.1 m severe dry; –0.1 to –0.05 m medium dry; –0.05 to –0.02 m mild dry; –0.02 to

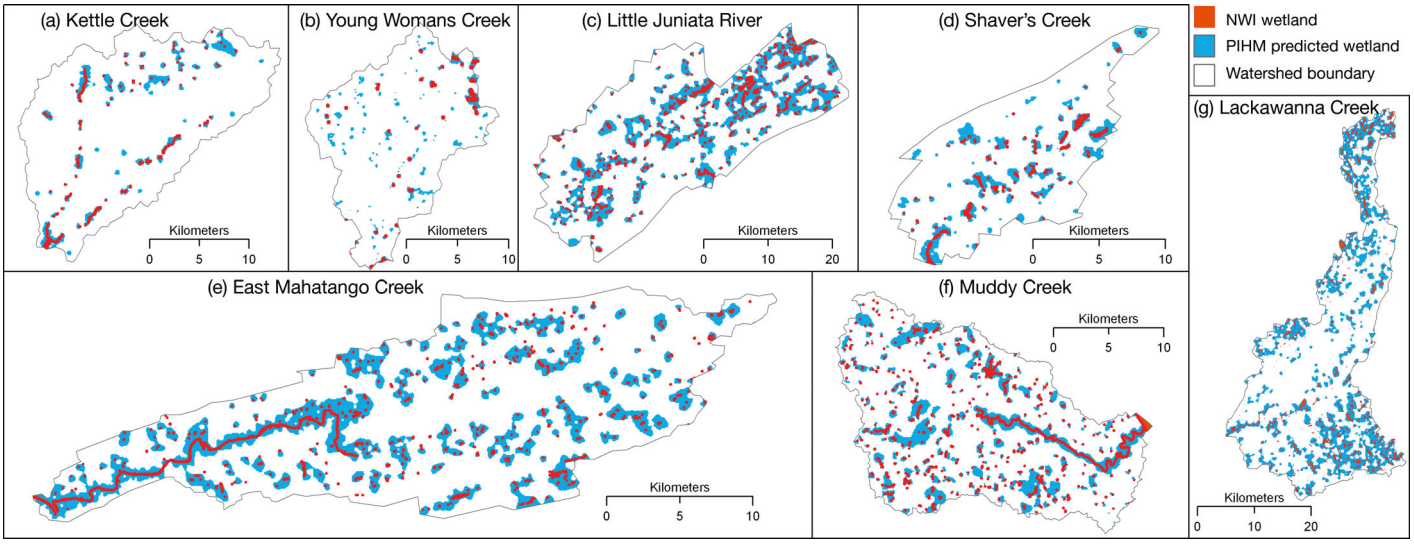

Fig. 7. National Wetlands Inventory (NWI) locations (red dots) and PIHM simulated shallow water table wetland areas (blue) during 2004 to 2010 for the 7 watersheds

Table 7. Basin-average large-scale response. ET: Evapotranspiration

Watershed	Precipitation (mm yr^{-1})		ET (mm yr^{-1})		Streamflow (mm yr^{-1})		Average water table elevation (m)	
	1979–1998	2046–2065	1979–1998	2046–2065	1979–1998	2046–2065	1979–1998	2046–2065
KC	1025	1124	395	433	522	616	2.06	2.02
YWC	1025	1124	281	312	618	732	2.89	2.85
LJR	1025	1124	425	468	545	652	3.44	3.39
SC	1025	1124	482	487	459	591	4.32	4.28
EMC	1025	1124	433	474	491	605	2.45	2.39
MC	1025	1124	243	261	611	716	4.38	4.35
LR	1025	1124	304	332	614	731	2.91	2.87

0.02 m no change; >0.02 m wet (Fig. 8). The grouped water table response is plotted in Fig. 9. We used Z-test to test if the water table response is not significantly different than zero (Table 8). The results suggested that the future water tables are different from historical water table at significance level 0.01. Clearly, groundwater in upland areas is more vulnerable to future climate.

5. DISCUSSION

5.1. How PIHM explains groundwater and stream water interaction

Coupled surface–subsurface hydrologic modeling discretizes the whole watershed into landscape grid elements. The water movement equations govern the groundwater-surface water exchange in each grid and lateral convergence between neighboring grids. This reveals the spatial dynamics that is hidden in the lumped runoff signal monitored at the catchment outlet. In the real-world application of coupled surface–subsurface models, appropriate calibration constraints are required to improve the simulation fidelity. Clearly, without considering water table depth during the calibration process, the model results might not be adequate for understanding the spatial near-surface hydrological dynamics (Ebel & Loague 2006). The addition of water table depth may also affect the general model performance. For example, the YWC and LJR were modeled by PIHM in a previous study (Yu et al. 2013); the NSE showed that the streamflow performance was poorer. This implies that the spatial constraint may cancel out the streamflow performance. In 6 of the watersheds, the

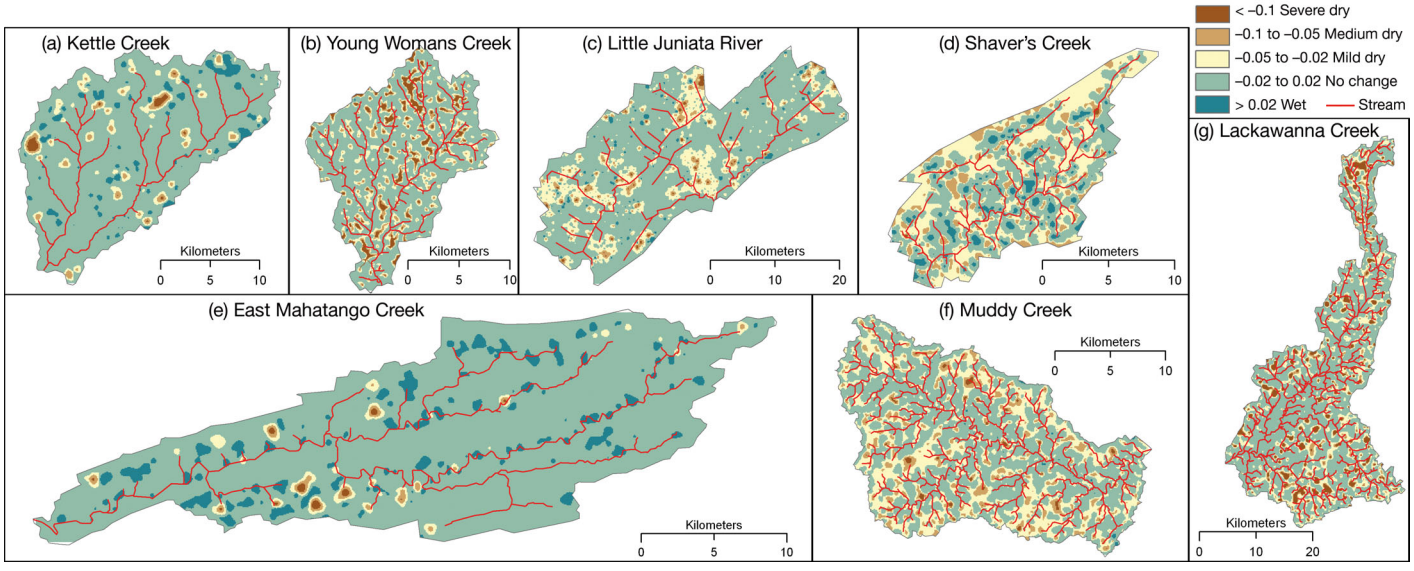

Fig. 8. Difference maps for the simulated groundwater table elevation between the climate scenario period 2046–2065 and the reference period 1979–1998 for the 7 watersheds. A negative/positive value indicates the region is drier/wetter under the climate change projection scenario. The color bar is selected based on the distribution of all the changes of groundwater table elevation (m).

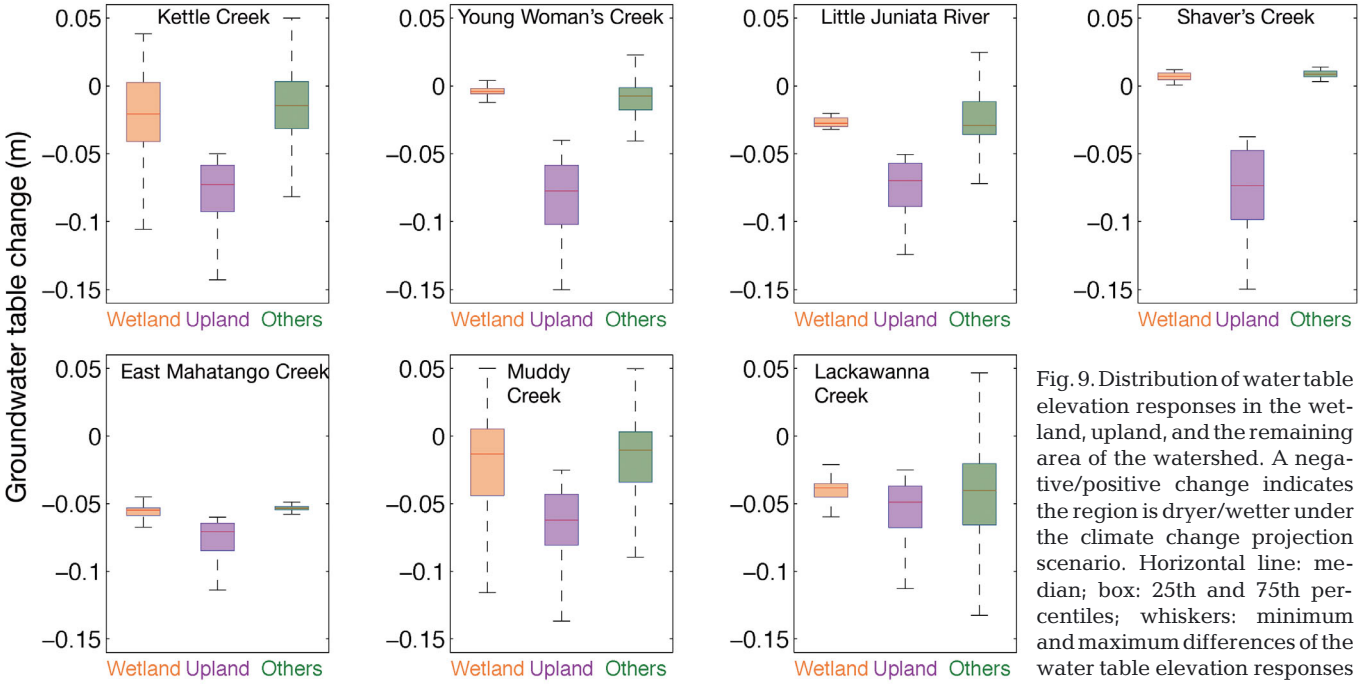

Fig. 9. Distribution of water table elevation responses in the wetland, upland, and the remaining area of the watershed. A negative/positive change indicates the region is dryer/wetter under the climate change projection scenario. Horizontal line: median; box: 25th and 75th percentiles; whiskers: minimum and maximum differences of the water table elevation responses

Table 8. Water table responses (m, mean ± SE) (plotted in Fig. 9). A negative/positive change indicates the region is dryer/wetter under the climate change projection scenario. The water table responses are significant at 0.01 level (Z-test)

Watershed	Wetland	Upland	Others
KC	−0.0257 ± 0.0019	−0.0803 ± 0.0013	−0.0175 ± 0.0006
YWC	−0.0310 ± 0.0002	−0.0840 ± 0.0017	−0.0094 ± 0.0006
LJR	−0.0333 ± 0.0005	−0.0746 ± 0.0032	−0.0262 ± 0.0011
SC	0.0132 ± 0.0014	−0.0773 ± 0.0032	0.0189 ± 0.0007
EMC	−0.0559 ± 0.0008	−0.0795 ± 0.0010	−0.0504 ± 0.0005
MC	−0.0225 ± 0.0011	−0.0645 ± 0.0012	−0.0191 ± 0.0006
LR	−0.0428 ± 0.0004	−0.0554 ± 0.0009	−0.0429 ± 0.0006

streamflow performance was satisfactory (i.e. NSE > 0.50 and ME < ±25% [Moriasi et al. 2007]), which suggested that it is reasonable and practical to add groundwater constraints according to wetland distribution in NWI. The PIHM streamflow simulation does not perform well at LR. This could be due to the large NWI wetland coverage (Table 2) in LR, which led to overwhelming spatial constraints in Eq. (6). Finally, the calibration did not lead to satisfactory streamflow performance (NSE > 0.5).

Due the limited data regarding the subsurface, we applied a uniform subsurface layer for all the watersheds. A 5 m depth was assumed as the bottom boundary of shallow groundwater throughout the whole watershed. A large-scale groundwater modeling study (Fan et al. 2013) suggested that shallow groundwater depth in the SRB is around 0 to 40 m. In LJR, another PIHM modeling study used 40 m as the uniform subsurface layer (Kumar, 2009). Here, we focus only on the top 0.3 m dynamics. The spatially distributed wetland locations are well predicted by PIHM simulation (Table 6). Also the temporal validation of the streamflow performance (Fig. 6, column 3) is consistent with the performance during calibration period (Fig. 6, column 2). We argue that though the absolute water table depth is definitely not perfectly simulated across each watershed, the dynamics of water table fluctuation is captured with a 5 m subsurface layer, and this is enough to identify the freshwater wetland. It will be interesting to examine the role of subsurface complexity in modeling surface runoff and shallow groundwater dynamics.

Our study focused in particular on data availability, hydrologic model behavior constraints, wetland hydrology interpretation, and spatial heterogeneity of water table dynamics. This is especially important for data and model applications in the framework of national databases (Duffy et al. 2011). Furthermore, temporal and spatial wetland dynamics modeling using a hydrological modeling-driven method provides an alternative for wetland ecosystem management (Brooks & Wardrop 2013).

5.2. Differences between NWI and hydrologic identification

The NWI maps are prepared through conventional photointerpretation techniques, as well as through field checks (Tiner 2002). Studies have shown that if an NWI map indicates the presence of a wetland in a given area, it is highly likely that a wetland is there (Johnston & Meysembourg 2002, Kudray & Gale 2000, Maxa & Bolstad 2009). Conversely, if an NWI map does not indicate a wetland, there is quite a high probability that one is not there, but nevertheless, one can still find unmapped wetlands on the ground, particularly in favorable landscape positions such as along streams in narrow valleys or in depressions (Tiner 2002). Many of the wetlands in these landscape positions may also be forested, leading to under-representation in the NWI. For example, in the Upper Juniata watershed, a probability-based survey allowed us to ascertain that the NWI represented only 54% of the total wetland resource (Wardrop et al. 2007b). Model simulated wetlands preserved the spatial water table depth pattern and also provided a likely mapping for exploring missing wetlands in the NWI, which was consistent with the conclusion that NWI maps tend to err more by omission that by commission (Tiner 2002). Future study may validate the authenticity of the un-mapped wetland area.

5.3. Groundwater level response at a local and large (basin-averaged) scale

In the SRB, the average groundwater level response to climate change was subtle due to the combined effects of increased precipitation and increased evapotranspiration. Distributed modeling enabled the analysis of regional or local scale groundwater level changes controlled by land cover, soil, topography, etc. For example, this study identified different behavior in wetlands and uplands. In general, the model results suggested that the upland groundwater level was more sensitive to climate change than the wetland groundwater level. This may be due to the lateral redistribution of groundwater flow in PIHM. If this simulated heterogeneity of water table responses is correct, local field monitoring data of groundwater tables at wetlands only will lead to a biased conclusion about the climate change responses. For example, if one were to monitor limited locations of wetland water tables, one would conclude there was no change, which would not provide a complete picture of the watershed as a whole. Notably, if the decrease in upland groundwater level continues for a long time period, it will eventually affect the rest of the watershed including wetland areas.

5.4. Uncertainty in climate project and spatial hydrologic prediction

An important issue when considering adaption and mitigation of hydrologic responses to climate change is uncertainty. Due to the uncertainty of climate models, it is robust to use multiple greenhouse gas emission scenarios from multiple climate models (e.g. Chen et al. 2011, Benčoková et al. 2011, Masood et al. 2015). Due to the uncertainty of hydrological prediction, coupled surface–subsurface simulation is recommended to resolve potential spatial impacts due to the combined heterogeneity of topography, soil, land cover (e.g. Sulis et al. 2011). Both sources of uncertainty require computational resources. In this study, we focused on reducing spatial uncertainty in the prediction of the water table, which required coupled surface–subsurface simulation. Therefore we selected PIHM, a complex hydrologic model, with 2 coupled subsurface layers (saturated and unsaturated) and a spatially distributed computational mesh. Temporally, PIHM uses a fully implicit scheme to simulate continuous coupled surface–subsurface processes. Due to the computational expense of running PIHM, we used historical performance metrics and applied bias correction to force PIHM with only the best-performing climate model. This can be considered as a preliminary analysis of the sensitivity of spatial water table dynamics to climate change (Sulis et al. 2011). We demonstrated that PIHM is a potential tool for the simulation of spatial groundwater dynamics and assessment of wetland resources. The difference between basin scale response and regional scale response addressed the importance of resolving spatial hydrologic heterogeneity.

Notably, other sources of uncertainty, such as future vegetation resilience, societal priorities and land-use dynamics (Jones 2011), are all linked to the complex environmental system. The uncertainty related to climate projection scenarios, watershed spatial representation, and subsurface complexity remains an important area of future work.

6. CONCLUSIONS

In this study we present the first attempt to model the water table over 7 watersheds in the SRB to cap-

ture the hydrologic control of freshwater wetlands. The model application was made possible by a coupled surface–subsurface distributed hydrologic model, PIHM, that utilized a combination of spatial water table and streamflow constraints. We were able to predict spatial groundwater responses to future climate change. Scrutinizing the model performance and future climate responses reveals important insights in the distributed modeling of freshwater wetland dynamics:

(1) In general, the combined constraint of streamflow and spatial wetland location could lead to explicit hydrologic identification of wetland locations and area.

(2) PIHM not only reproduced the NWI located wetland, but also predicted extra wetland area, which provides a potential tool for verifying and improving the quality of the NWI map.

(3) Based on the selected best-performing climate model MRI-CGCM2.3.2, a future climate of increased precipitation and temperature will decrease the basin averaged water table elevation from 0.03 to 0.06 m.

(4) The shallow groundwater demonstrated complex responses to climate change, including a significant decrease in upland groundwater levels under the climate scenario for years 2046 to 2065 from MRI-CGCM2.3.2.

An important consideration when assessing wetland function is the temporal variability of hydrological regimes at daily to seasonal scales. From the coupled surface–subsurface modeling framework, temporal variability can be explicitily represented at shorter timescales for transpiration, soil moisture, lateral groundwater fluxes, etc. Wetland functions are closely tied to hydrologic flux and storage. The next step is to investigate the temporal signals of hydrologic conditions in these wetlands. Much more work is needed to evaluate the temporal dynamics of the wetlands and the associated ecological impacts.

Acknowledgements. The authors are grateful to the Associate Editor and 3 anonymous reviewers, who provided very detailed and constructive comments that improved the paper. This research was funded by grants from the US Environmental Protection Agency (EPA R833013 Hydrologic Forecasting for Characterization of Non-linear Response of Freshwater Wetlands to Climatic and Land Use Change in the Susquehanna River Basin), and from the US National Science Foundation (EAR 07-25019, EAR 12-39285, and EAR 13-31726 Shale Hills-Susquehanna Critical Zone Observatory, and IIS 13-44272).

LITERATURE CITED

Bhatt G, Kumar M, Duffy CJ (2014) A tightly coupled GIS and distributed hydrologic modeling framework. Environ Model Softw 62:70–84

Brooks RP, Wardrop DH (2013) Mid-Atlantic freshwater wetlands: advances in wetlands science, management, policy, and practice. Springer, New York, NY

Chen F, Dudhia J (2001) Coupling an advanced land surface-hydrology model with the Penn State-NCAR MM5 modeling system. I. Model implementation and sensitivity. Mon Weather Rev 129:569–585

Chen J, Brissette FP, Leconte R (2011) Uncertainty of downscaling method in quantifying the impact of climate change on hydrology. J Hydrol (Amst) 401:190–202

Chien H, Yeh PJF, Knouft JH (2013) Modeling the potential impacts of climate change on streamflow in agricultural watersheds of the Midwestern United States. J Hydrol (Amst) 491:73–88

Clark MP, Fan Y, Lawrence DM, Adam JC and others (2015) Improving the representation of hydrologic processes in Earth System Models. Water Resour Res 51:5929–5956

Cohen SD, Hindmarsh AC (1996) CVODE, a stiff/nonstiff ODE solver in C. Comput Phys 10:138–143

Delworth TL, Broccoli AJ, Rosati A, Stouffer RJ and others (2006) GFDL's CM2 Global Coupled Climate Models. 1. Formulation and simulation characteristics. J Clim 19: 643–674

Diansky NA, Volodin EM (2002) Simulation of present-day climate with a coupled atmosphere-ocean general circulation model. Izv Atmos Ocean Phys 38:732–747 (English translation)

Duffy C, Leonard L, Bhatt G, Yu X, Giles L (2011) Watershed reanalysis: towards a national strategy for model-data integration. IEEE 7th Int Conf, Stockholm, 5–8 Dec 2011. IEEE, New York, NY, p 61–65

Ebel BA, Loague K (2006) Physics-based hydrologic response simulation: seeing through the fog of equifinality. Hydrol Processes 20:2887–2900

Fan Y, Li H, Miguez-Macho G (2013) Global patterns of groundwater table depth. Science 339:940–943

Flato GM, Boer GJ (2001) Warming asymmetry in climate change simulations. Geophys Res Lett 28:195–198

Fossey M, Rousseau AN, Bensalma F, Savary S, Royer A (2015) Integrating isolated and riparian wetland modules in the PHYSITEL/HYDROTEL modelling platform: model performance and diagnosis. Hydrol Processes 29: 4683–4702

Furevik T, Bentsen M, Drange H, Kindem IKT, Kvamstø NG, Sorteberg A (2003) Description and evaluation of the Bergen Climate Model: ARPEGE coupled with MICOM. Clim Dyn 21:27–51

Golden HE, Lane CR, Amatya DM, Bandilla KW, Kiperwas HR, Knightes CD, Ssegane H (2014) Hydrologic connectivity between geographically isolated wetlands and surface water systems: a review of select modeling methods. Environ Model Softw 53:190–206

Gordon HB, Rotstayn LD, McGregor JL, Dix MR and others (2002) The CSIRO Mk3 Climate System Model. CSIRO Atmospheric Research Technical Paper 60, CSIRO Division of Atmospheric Research, Aspendale

Grayson RB, Blöschl G, Western AW, McMahon TA (2002) Advances in the use of observed spatial patterns of catchment hydrological response. Adv Water Resour 25: 1313–1334

Green TR, Taniguchi M, Kooi H, Gurdak JJ and others (2011) Beneath the surface of global change: impacts of climate change on groundwater. J Hydrol (Amst) 405: 532–560

Hansen N, Ostermeier A (2001) Completely derandomized self-adaptation in evolution strategies. Evol Comput 9: 159–195

Huntington TG (2003) Climate warming could reduce runoff significantly in New England, USA. Agric For Meteorol 117:193–201

Johnson WC, Boettcher SE, Poiani KA, Guntenspergen G (2004) Influence of weather extremes on the water levels of glaciated prairie wetlands. Wetlands 24:385–398

Johnston CA, Meysembourg P (2002) Comparison of the Wisconsin and national wetlands inventories. Wetlands 22:386–405

Jones JA (2011) Hydrologic responses to climate change: considering geographic context and alternative hypotheses. Hydrol Processes 25:1996–2000

Jungclaus JH, Keenlyside N, Botzet M, Haak H and others (2006) Ocean circulation and tropical variability in the coupled model ECHAM5/MPI-OM. J Clim 19:3952–3972

K-1 Model Developers (2004) K-1 Coupled GCM (MIROC) description. K-1 Technical Report (Hasumi H, Emori S eds), Center for Climate System Research, University of Tokyo

Kløve B, Ala-Aho P, Bertrand G, Gurdak JJ and others (2014) Climate change impacts on groundwater and dependent ecosystems. J Hydrol (Amst) 518:250–266

Kudray GM, Gale MR (2000) Evaluation of national wetland inventory maps in a heavily forested region in the upper great lakes. Wetlands 20:581–587

Kumar M (2009) Toward a hydrologic modeling system. PhD dissertation, The Pennsylvania State University, State College, PA

Kumar M, Marks D, Dozier J, Reba M, Winstral A (2013) Evaluation of distributed hydrologic impacts of temperature-index and energy-based snow models. Adv Water Resour 56:77–89

Legutke S, Voss R (1999) The Hamburg atmosphere-ocean coupled circulation model ECHO-G. Technical Report 18, German Climate Computer Centre (DKRZ), Hamburg

Li H, Sheffield J, Wood EF (2010) Bias correction of monthly precipitation and temperature fields from Intergovernmental Panel on Climate Change AR4 models using equidistant quantile matching. J Geophys Res 115:1–20

Lu J, Sun G, McNulty SG, Comerford NB (2009) Sensitivity of pine flatwoods hydrology to climate change and forest management in Florida, USA. Wetlands 29:826–836

Martin GI, Kirkman LK, Hepinstall-Cymerman J (2012) Mapping geographically isolated wetlands in the Dougherty Plain, Georgia, USA. Wetlands 32:149–160

Masood M, Yeh PF, Hanasaki N, Takeuchi K (2015) Model study of the impacts of future climate change on the hydrology of Ganges–Brahmaputra–Meghna basin. Hydrol Earth Syst Sci 19:747–770

Maxa M, Bolstad P (2009) Mapping northern wetlands with high resolution satellite images and LiDAR. Wetlands 29: 248–260

McLaughlin DL, Kaplan DA, Cohen MJ (2014) A significant nexus: geographically isolated wetlands influence landscape hydrology. Water Resour Res 50:7153–7166

Meehl GA, Covey C, Delworth T, Latif M and others (2007) The WCRP CMIP3 multi-model dataset: a new era in climate change research. Bull Am Meteorol Soc 88: 1383–1394

Mesinger F, DiMego G, Kalnay E, Mitchell K and others (2006) North American regional reanalysis. Bull Am Meteorol Soc 87:343–360

Min JH, Wise WR (2009) Simulating short-circuiting flow in a constructed wetland: the implications of bathymetry and vegetation effects. Hydrol Processes 23:830–841

Mirus BB, Loague K (2013) How runoff begins (and ends): characterizing hydrologic response at the catchment scale. Water Resour Res 49:2987–3006

Moriasi DN, Arnold JG, Van Liew MW, Bingner RL, Harmel RD, Veith TL (2007) Model evaluation guidelines for systematic quantification of accuracy in watershed simulations. Trans ASABE 50:885–900

Najjar R, Patterson L, Graham S (2009) Climate simulations of major estuarine watersheds in the Mid-Atlantic region of the US. Clim Change 95:139–168

Najjar RG, Pyke CR, Adams MB, Breitburg D and others (2010) Potential climate-change impacts on the Chesapeake Bay. Estuar Coast Shelf Sci 86:1–20

NASA (2013) LDAS Land Data Assimilation Systems: NLDAS-2 forcing dataset information. http://ldas.gsfc.nasa.gov/nldas/NLDAS2forcing.php

Nash JE, Sutcliffe JV (1970) River flow forecasting through conceptual models. I. A discussion of principles. J Hydrol (Amst) 10:282–290

NRC (National Research Council) (1995). Wetlands: characteristics and boundaries. National Academy Press, Washington, DC

Neff R, Chang H, Knight CG, Najjar RG, Yarnal B, Walker HA (2000) Impact of climate variation and change on Mid-Atlantic Region hydrology and water resources. Clim Res 14:207–218

Ozesmi SL, Bauer ME (2002) Satellite remote sensing of wetlands. Wetlands Ecol Manag 10:381–402

Pyzoha JE, Callahan TJ, Sun G, Trettin CC, Miwa M (2008) A conceptual hydrologic model for a forested Carolina bay depressional wetland on the coastal plain of South Carolina, USA. Hydrol Processes 22:2689–2698

Qu Y, Duffy CJ (2007) A semidiscrete finite volume formulation for multiprocess watershed simulation. Water Resour Res 43, W08419, doi:10.1029/2006WR005752

Reichler T, Kim J (2008) How well do coupled models simulate today's climate? Bull Am Meteorol Soc 89:303–311

Rogers CE, McCarty JP (2000) Climate change and ecosystems of the Mid-Atlantic Region. Clim Res 14:235–244

Salas-Mélia D, Chauvin F, Déqué M, Douville H and others (2005) Description and validation of the CNRM-CM3 Global Coupled Model. CNRM Working Note 103, Centre National de Recherches Météorologiques, Toulouse

Scibek J, Allen DM (2006) Modeled impacts of predicted climate change on recharge and groundwater levels. Water Resour Res 42:W11405, doi:10.1029/2005WR004742

Smardon RC (2009) Sustaining the world's wetlands: setting policy and resolving conflicts. Springer, New York, NY

Su M, Stolte WJ, Van der Kamp G (2000) Modelling Canadian prairie wetland hydrology using a semi-distributed streamflow model. Hydrol Processes 14:2405–2422

Sulis M, Paniconi C, Rivard C, Harvey R, Chaumont D (2011) Assessment of climate change impacts at the catchment scale with a detailed hydrological model of surface–subsurface interactions and comparison with a land surface model. Water Resour Res 47:W01513, doi:10.1029/2010WR009167

Taylor RG, Scanlon B, Doll P, Rodell M and others (2013) Ground water and climate change. Nat Clim Change 3: 322–329

Tiner RW (2002) Wetland indicators: a guide to wetland identification, delineation, classification, and mapping.

CRC Press, Boca Raton, FL

US Army Corps of Engineers and EPA (2015) Clean Water Rule: definition of 'waters of the United States'. Fed Regist 80:37054–37127

Wang L, Chen W (2014) Equiratio cumulative distribution function matching as an improvement to the equidistant approach in bias correction of precipitation. Atmos Sci Lett 15:1–6

Wardrop DH, Kentula ME, Jensen SF, Stevens DL, Hychka KC, Brooks RP (2007a) Assessment of wetlands in the Upper Juniata Watershed in Pennsylvania, USA using the hydrogeomorphic approach. Wetlands 27:432–445

Wardrop DH, Kentula ME, Stevens DL, Jensen SF, Brooks RP (2007b) Assessment of wetland condition: an example from the Upper Juniata Watershed in Pennsylvania, USA. Wetlands 27:416–431

Yu X, Bhatt G, Duffy CJ, Shi Y (2013) Parameterization for distributed watershed modeling using national data and evolutionary algorithm. Comput Geosci 58:80–90

Yuan LR, Xin P, Kong J, Li L, Lockington D (2011) A coupled model for simulating surface water and groundwater interactions in coastal wetlands. Hydrol Processes 25: 3533–3546

Yukimoto S, Noda A, Kitoh A, Sugi M and others (2001) The New Meteorological Research Institute coupled GCM (MRI-CGCM2): model climate and variability. Pap Meteorol Geophys 51:47–88

Zhang Z, Dehoff AD, Pody RD, Balay JW (2010) Detection of streamflow change in the Susquehanna River Basin. Water Resour Manag 24:1947–1964

Editorial responsibility: Bryson Bates, Wembley, WA, Australia

Submitted: November 20, 2014; Accepted: October 13, 2015
Proofs received from author(s): November 20, 2015